Microstructure of vertebrae, ribs, and gastralia of Triassic sauropterygians – New insights into the microanatomical processes involved in aquatic adaptations of marine reptiles

Nicole Klein[1*], Aurore Canoville[2], and Alexandra Houssaye[3]

[1]Steinmann Institute, Paleontology, University of Bonn, Nussallee 8, 53115 Bonn, Germany.

[2] Department of Biological Sciences, North Carolina State University & Paleontology, North Carolina Museum of Natural Sciences, 11 W. Jones St, Raleigh, NC 27601, USA.

[3]UMR 7179 CNRS/Muséum National d'Histoire Naturelle, Département Adaptations du Vivant, 57 rue Cuvier CP-55, 75005 Paris, France.

*Tel:+49-228-7360043; Fax: +49-228-73-3509; Email: nklein@posteo.de.

Running title: Microanatomy of Triassic Sauropterygia

This article has been accepted for publication and undergone full peer review but has not been through the copyediting, typesetting, pagination and proofreading process which may lead to differences between this version and the Version of Record. Please cite this article as doi: 10.1002/ar.24140

ABSTRACT

Isolated ribs and vertebrae of Middle Triassic sauropterygians are studied. The vertebrae have a well-defined large cavity in their centra, which is a unique feature and is without any modern analogue. The articular facets of vertebrae are made of endochondral bone including calcified as well as uncalcified cartilage. Vertebrae are pachyosteosclerotic in the pachypleurosaurs *Neusticosaurus* and *Serpianosaurus* from the Alpine Triassic, and osteosclerotic in the placodont, in the medium-sized *Nothosaurus marchicus*, and in the pachypleurosaur *Anarosaurus*. In large *Nothosaurus* specimens, the vertebrae are cavernous.

The ribs of all sampled specimens are osteosclerotic, which resembles the microanatomy of long bones in all studied taxa. The proximal to medial part of ribs mainly consist of a compact periosteal cortex surrounding an inner endosteal territory. Towards the distal end of the ribs, the periosteal thickness decreases whereas the endosteal territory increases. Despite a shift from periosteal vs. endosteal tissues, global rib compactness remains relatively constant.

Osteosclerosis in ribs and vertebrae is reached by the same processes as in the long bones: by a relative increase in cortex thickness that is coupled by a reduction of the medullary cavity, by the persistence of calcified cartilage, and by an inhibition of remodelling although some resorption may occur but without complete redeposition of bone. Processes differ from those observed in Permian marine reptiles and some mosasaurines, where either extensive remodelling or inhibition of bone resorption leads to osteosclerosis.

Besides differences regarding the microanatomy, all studied bones of a taxon are consistent in their bone tissue type.

Key words: pachyosteosclerosis, osteosclerosis, inhibition of remodelling**,** central cavity in centra, ribs with consistent global compactness

INTRODUCTION

During the Early and Middle Triassic, numerous tetrapod groups reinvaded the marine realm, thus developing convergent adaptations to an aquatic lifestyle. Sauropterygia was one diverse group of diapsid marine reptiles that existed from the late Early Triassic to the end of the Cretaceous (Motani, 2009; Rieppel, 2000). Their Triassic radiation was restricted to near-shore habitats of the Tethys Ocean and connected epicontinental seas (Rieppel, 2000). It thus primarily involved coastal and shallow marine forms of Placodontia, Pachypleurosauria, Nothosauroidea, and Pistosauroidea; the latter three clades forming the Eosauropterygia (Rieppel, 2000). In the deposits of the Germanic Basin of Central Europe (i.e. Muschelkalk layers/units), individual numbers of Eosauropterygia are high. However, most skeletal remains are found in bonebeds and condensation horizons (e.g., Meyer, 1847-55; Rieppel, 2000; Schröder, 1914) and are thus usually highly disarticulated and/or isolated. Thus, the taxonomical assignment of these isolated bones beyond family level is often difficult (e.g., Klein et al., 2015a, 2016a; Rieppel, 2000).

In the course of secondary adaptation to an aquatic lifestyle, a given lineage will undergo numerous changes affecting, for example, its locomotion and buoyancy, sensors, salinity/osmoregulation, feeding strategy and diet, reproduction, as well as air regulation during

diving (see Houssaye and Fish, 2016; Thewissen and Nummela, 2008). Besides gross-morphological changes affecting the skeleton, the microstructure (i.e., inner structure) of skeletal elements is also affected due to changing requirements in locomotion and buoyancy. Bone microanatomy, i.e., the amount and distribution of the osseous tissue in the bone, is strongly associated with lifestyle and bone biomechanics (e.g. Canoville and Laurin, 2009, 2010; Canoville et al., 2016; Dumont et al., 2013; Houssaye et al., 2010, 2014; Quemeneur et al., 2013) and can thus indicate ecological preferences (e.g. Buffrénil et al., 1987, 1990; Germain and Laurin, 2005; Houssaye et al., 2013, 2015; Laurin et al., 2004, 2007, 2011). Further on, changes of microanatomical patterns during the evolutionary history of a clade can document processes of secondary aquatic adaptations (e.g. Amson et al., 2014; Buffrénil et al., 2010; Houssaye et al., 2015).

Aquatic tetrapods display two main types of microanatomical specializations (e.g., Amson et al., 2014; Buffrénil et al., 2010; Canoville and Laurin, 2010; Hayashi et al., 2013; Houssaye et al., 2013, 2016; Ricqlès and Buffrénil, 2001) resulting in bone mass increase (BMI) or bone mass decrease (BMD) as compared to the plesiomorphic terrestrial phenotype. BMD results in the acquisition of a spongious inner-architecture of skeletal elements and an overall lightening of the skeleton. This spongious organization is typical for active swimmers requiring high speed and manoeuvrability in open water habitats (Buffrénil et al., 1986; Buffrénil and Mazin, 1990; Houssaye et al., 2014; Ricqlès and Buffrénil, 2001). BMI acts as a ballast to counteract positive buoyancy and is typical for shallow marine forms being slow swimmers and

divers, and/or taxa at an initial stage of adaptation to an aquatic environment (Amson et al., 2014; Buffrénil et al., 2010; Houssaye, 2009, 2013; Houssaye et al., 2015, 2016). BMI is the outcome of two independent processes that can be coupled or not, general or localized in the skeleton: i) osteosclerosis that corresponds to an inner bone compaction of the skeletal element, accompanied by a reduction of the medullary cavity, as compared to the plesiomorphic terrestrial phenotype; ii) pachyostosis that is an hyperplasy of bone periosteal cortices (extended centrifugal growth of the periosteal cortex), affecting the gross-morphology (swollen aspect) of the skeletal elements (Buffrénil et al., 2010; Houssaye, 2009). However, these contrasting patterns are not mutually exclusive and can be variously combined between different elements of the skeleton (Buffrénil et al., 2010; Houssaye et al., 2016). Inversions in trends of skeletal density can occur during the evolutionary history of a given clade and are usually associated to ecological changes (e.g., cetaceans, mosasaurs; Buffrénil and Mazin, 1990; Houssaye et al., 2013, 2015; Ricqlès and Buffrénil, 2001). Different skeletal regions (appendicular and axial) can exhibit similar microanatomical adaptations (e.g., Amson et al., 2018; Dewaele et al., 2018) and thus a congruent ecological signal, although this is not always the case (Houssaye et al., 2016).

Microstructural adaptations to an aquatic lifestyle have been extensively studied in the limb bones of various tetrapod clades (e.g., Canoville et al., 2010; Ksepka et al., 2015), and to a lesser extent in the axial skeleton (mostly vertebrae and ribs, Amson et al., 2014; Buffrénil et al., 1990; 2008, 2010; Canoville et al., 2016; Dumont et al., 2013; Gray et al., 2007; Houssaye, 2008; Houssaye and Bardet, 2012; Houssaye et al., 2015). For Triassic sauropterygians, previous

works have primarily focused on the histology and microanatomy of long bones (Buffrénil and Mazin, 1992; Hugi, 2011; Hugi et al., 2011; Klein, 2010; Klein and Griebeler, 2016, 2018; Klein et al., 2015b, 2016b; Krahl et al., 2013; Sander, 1990). These studies have shown that bone tissue types of Triassic Sauropterygia can be generally categorized as lamellar-zonal or fibrolamellar. However, these marine reptiles exhibit an enormous diversity of bone tissues as well as combinations of tissues, varying vascular densities, as well as diverse microanatomical patterns, which are to this extent unknown in any extant tetrapod group (see references above).

A comprehensive study of the vertebral and rib microanatomy of these groups is lacking. The current study thus aims at describing the rib and vertebral microanatomy and histology of some Triassic sauropterygians. Further on, comparisons with their long bone microstructure and with other taxa are conducted, in order to better understand their skeletal adaptations to an aquatic lifestyle.

Abbreviations

NMNHL RGM (Wijk), National Museum of Natural History Naturalis, Leiden, The Netherlands; PIMUZ, Paleontological Institute and Museum of the University of Zurich, Switzerland; SMNS, State Museum of Natural History Stuttgart, Germany; StIPB, Steinmann-Institute, Division of Paleontology, University of Bonn, Germany.

MATERIAL AND METHODS

The sampled ribs, gastralia, and vertebrae originate from the locality of Winterswijk (The Netherlands; Anisian), from classical Muschelkalk and Lettenkeuper localities in southern Germany (early and late Ladinian), and from the Alpine Triassic of Monte San Giorgio (Anisian/Ladinian) (Table 1).

All ribs and vertebrae were found in isolation except for the nothosaur rib SMNS 80266, which belongs to a disarticulated but nearly complete individual of *Nothosaurus* sp. (pers. com. D. Seegis, 2016/SMNS). All respective thin sections are curated under the collection numbers given in Table 1. Some thin sections were newly made for this study; others were already in the collections of the SMNS (unpublished master thesis of Weidemeyer, 2001 at the GPIT) or of the PIMUZ (Hugi et al., 2011; Hugi, 2011; Hugi unpublished material). If not mentioned otherwise, sampled ribs are usually mid-dorsal ribs and vertebrae represent dorsal vertebrae.

The morphology of eosauropterygian ribs and vertebrae is not diagnostic. An accurate taxonomical assignment based on morphology is thus not possible but also beyond the scope of this paper, which intends to focus on trends in histology and microanatomy of ribs and vertebrae for this group. However, based on characteristic tissue types and overall microanatomy, a taxonomical identification was sometimes possible (Table 1). Indeed, ribs and vertebrae are clearly pachyostotic in placodonts and in all Eosauropterygia from the Alpine Triassic: i.e., the pachypleurosaurs *Neusticosaurus* spp. and *Serpianosaurus* as well as the nothosaurs *Lariosaurus*/*Ceresiosaurus* (summarized in Rieppel, 2000). Vertebrae and the proximal part of

ribs appear usually somewhat swollen in other Eosauropterygia (i.e. *Anarosaurus*, *Nothosaurus marchicus*, pistosauroid) but are not pachyostotic when compared to those of the above-mentioned taxa.

The ribs and vertebrae were photographed and measured before destructive sampling (Table 1). Transverse sections of the ribs were cut along their shaft (perpendicular to the long axis of the element) to document microanatomical variation along the length of the rib from the proximal to the distal end. Vertebrae were usually cut transversally except for one that was cut longitudinally. The thin sections were produced following standard petrographic methods (Klein and Sander, 2007), scanned with an Epson V740 PRO high-resolution scanner, and studied and photographed with a Leica1DM 750P compound polarizing microscope equipped with a digital camera (Leica1ICC50HD). The bone histological terminology follows Francillon-Vieillot et al. (1990).

RESULTS

Vertebrae

Gross morphology

In Eosauropterygia, the neurocentral suture, i.e., the connection between the centrum and the neural arch, is typically not fused in adults (skeletal paedomorphosis), contrary to placodonts were both are usually fused (see Rieppel, 2000). The neural arch pedicels are expanded at their

base resulting in a characteristic butterfly-shaped or cruciform facet, which makes the identification of isolated sauropterygian centra and/or neural arches easy (Rieppel, 2000:fig. 5). The vertebral centra are slightly constricted ventrally and laterally (except in some strongly pachyostotic taxa). Neural spines are low in pachypleurosaurs (e.g., Rieppel, 1989; Sander, 1989) and some nothosaurs (*Nothosaurus marchicus*, *N. giganteus*) but high in others (*N. mirabilis*) (Rieppel, 2000; Klein et al., 2015a; Sander et al., 2014). However, the height of the neural arch depends also on the anatomical position of the vertebra.

Microanatomical features

The longitudinal section of the dorsal centrum (Wijk08-47) shows that the periosteal (dorsal and ventral cones) and endochondral (anterior and posterior cones) territories (see Buffrénil et al., 2008 for details) are clearly distinct, the cones of periosteal origin being much more compact (Fig. 1A). The layer of compact cortex is thicker in the dorsal cone than in the ventral one. Around the growth center, resorption occurred, resulting in large cavities scattered around the core of the centrum. Away from the sagittal plane, resorption is more important in the ventral cone of periosteal origin so that all this area becomes spongious, whereas the dorsal cone remains strongly compact.

In transverse section, the compact bone surrounds most of the periphery of the vertebra (i.e., the dorsal part of the neural arch, including the neural spine, the inner margin of the neural canal, and the ventrolateral margin of the centrum). The layer can be rather thin, like in the

centrum and neural arch of Wijk10-535 (Fig. 1C) or thick, like in the centrum of Wijk08-94 (Fig. 1D) and in the neural arch of Wijk13-88 (Fig. 1B). The zones of articulation (articular facets between neural arch and centrum as well as laterally where the ribs articulate) are spongious except in *Serpianosaurus* and *Neusticosaurus* (Figs. 1, 2). The centrum comprises a large central cavity, most likely corresponding to the former notochord, except in Wijk10-535, SMNS 54418, and *Serpianosaurus*. The centrum is crossed by trabeculae in Wijk10-535 (Fig. 1C) and filled by endosteal bone and dense calcified cartilage in *Serpianosaurus*, resulting in an extremely compact vertebra in the latter (Fig. 1G). Some endosteal trabeculae reach into the centrum cavities of Wijk08-94, Wijk08-126, and in that of *Neusticosaurus* (Figs. 1D, E, H, I). Vertebrae of pachypleurosaur *Neusticosaurus edwardsii* are less compact when compared to that of *Serpianosaurus* due to a strong radial vascularization (Figs. 1H, I). Additionally, around the articular facets some resorption occurred in *Neusticosaurus*, resulting in some erosion cavities. In SMNS 54418, the centrum consists of a spongiosa made of small trabeculae surrounded by a layer of compact bone (Fig. 1F). The neural arch and spine are in this sample compact, too, except for a central cavity in mid-line with the neural spine. This specimen results from a natural break and not from true sectioning.

StIPB R 68a and StIPB R 52, both from large *Nothosaurus* (*N. mirabilis* or *N. giganteus*), differ from the smaller eosauropterygian vertebrae in being generally less compact. They show a large central cavity in the centrum as well as several cavities in the neural arch (Fig. 1J),

resulting in an overall cavernous structure. A thin layer of compact bone surrounds the entire vertebrae as well as these inner cavities.

The placodont sample StIPB R 68b has a much thicker periosteal cortex around a relatively small central, triangular shaped cavity in the centrum with a small ring of endosteal bone in its center, forming a small pipe (Fig. 1K). One leg of the triangle reaches down to the ventral bone surface, the other extends only half way down, which might be an artifact of sampling location. Only one half of the neural arch is preserved that exhibits a large cavity, which is surrounded by two layers of periosteal bone, a thin one along the neural canal and a thicker one along the periphery.

Histological features

Bone tissue of the placodont vertebra (StIPB R68b) differs from that of the other described vertebrae by the occurrence of true fibro-lamellar bone with essentially radially oriented vascular canals organized in circumferential layers and a locally occurring primary trabecular structure (Figs. 2A-C), resulting in an overall spongious structure.

Primary bone tissue in the pachypleurosaurs *Neusticosaurus* and *Serpianosaurus* from the Alpine Triassic is made of well (*Neusticosaurus*) and low (*Serpianosaurus*) vascularized highly organized parallel-fibred bone. Vascular canals are simple and are arranged radially or longitudinally in circumferential rows (Figs. 1G-I).

The primary periosteal bone tissue of *Nothosaurus* is essentially made of parallel-fibred bone with a moderate vascular density (Figs. 2D-F). Vascular canals are simple, incompletely lined or can appear locally as primary osteons (Klein, 2010; Klein et al., 2016b). A longitudinal and radial orientation dominates. Locally, there is a tissue with much larger osteocyte lacunae that are also randomly shaped and sized, but that shows an extinction pattern in polarized light similar to that of parallel-fibered bone (Figs. 2H, I). This tissue thus is comparable to the unusual parallel-fibered bone evoked by Houssaye et al. (2013) in mosasaurs. This kind of parallel-fibred bone probably represents an intermediate stage between parallel-fibered and fibrous/woven bone (Klein and Griebeler, 2016). Locally, in combination with the occurrence of primary osteons, it results in incipient fibro-lamellar bone sensu Klein (2010).

The tissue of the regions of the articular facets (between neural arch and centrum as well as laterally where the ribs articulate) shows endochondral bone consisting essentially of calcified cartilage enclosed by endosteal trabeculae of varying thickness (thickest in the placodont and in large nothosaurs) or scattered with intertrabecular spaces lined by thin layers of endosteal bone (Figs. 1E, 2K-O). The placodont vertebra shows a network of endosteal trabeculae enclosing calcified cartilage, which is in a lesser extend also the structure of the articular regions in large nothosaur vertebrae. A trabecular structure of the endosteal tissue is not observed in small and medium sized eosauropterygians. The connective area between the endochondral territories of the centrum and the neural arch consists of uncalcified cartilage (Fig. 2O). Remodeling of periosteal bone was not observed in any of the samples. Only some resorption is documented in

the placodont vertebra in form of enlargement of primary osteons. In the samples where the neural spines are preserved, they are avascular (Figs. 1B, C).

Growth marks are common in periosteal regions of the vertebral centra with the succession of zones and annuli, and sometimes the addition of a true LAG (Figs. 2A, D, H, K). At the (dorsolateral) limit of the regions of periosteal and endochondral origin in the centrum, there are long distinct Sharpey's fibers (Fig. 2P).

Ribs

Gross morphology

A dorsal rib can morphologically be divided into the rib head, the usually curved proximal part, the only slightly curved or straight medial part, and the flat but broad distal part (Fig. 3B). This division was followed for sampling and study of the inner structure. Rib cross sections document the shape changes during ontogeny as a result of elongation and a posterior extension of the rib (Fig. 3). Cervical ribs of Sauropterygia are double headed whereas dorsal and sacral ribs are holocephalous (Rieppel, 2000).

Microanatomical features

Changes in the overall microstructure along the rib shaft are documented for all studied Sauropterygia (Figs. 3-6), as was observed in other amniotes. The rib head and the proximal part of the rib shaft generally display a thick and compact layer of periosteal bone that surrounds a

small medullary cavity or medullary region. From the medial part of the rib towards its distal end, the relative size of the medullary region increases whereas the relative thickness of the primary periosteal cortex decreases. The latter is reduced to a very thin layer in the distal part of all studied ribs. The structure and size of the medulla varies considerably between different samples, as well as along the shaft of a single rib (Table 1; Fig. 3). The medullary region is usually as compact as the periosteal region due to the persistence of calcified cartilage (Figs. 3, 5).

Only a few samples have at the proximal part of the rib a medullary cavity containing no or only a few bone trabeculae (Fig. 3B1). Others exhibits a small, not centred medullary cavity (Figs. 3D1, E1, 5D, E,) to a moderately (Figs. 3F1, G1) or large-sized medullary region (Figs. 3A1, 5A, B, F-H). SMNS 54434 (Fig. 3C1) is the only sample that has proximally a de-central, round medullary region filled solely by calcified cartilage. In the medial part of the rib a medullary region made by endosteal bone and calcified cartilage is present in all samples (Figs. 3A2-3, C2, D3-5, E2-3, F2, G2-3, 5J), except for Wijk07-31 where a cavity is retained but surrounded and crossed by trabeculae (Figs. 3B3-6). In the distal ends of all sampled ribs, the periosteal compact bone tissue is reduced and most of the section consist of the medullary territory that is occupied by endosteal bone, sometimes forming trabeculae, and calcified cartilage (Figs. 3A4, B7-8, C3, D5-6, E4, F3, G4, 5C, K-O).

Histological features

In all samples simple vascular canals and primary osteons are longitudinally and radially organized. The periosteal bone of the placodont rib **(**Wijk16-GG; Figs. 4A-C) consists of fibrolamellar bone tissue, which is however, less vascularized than in the vertebra (StIPB 68b, Figs. 1K, 2A-C) but much higher vascularized than in studied Eosauropterygia. Primary osteons in the placodont rib are locally enlarged by resorption (Figs. 4A, B).

Primary bone tissues in ribs of studied pachypleurosaurs are of variable nature. It consists of well, radially vascularized parallel-fibred bone tissue in *Neusticosaurus* (Fig. 6F), and of low to nearly avascular parallel-fibred and/or lamellar bone in *Serpianosaurus* (Figs. 6A-I).

The ribs of the large *Nothosaurus* (SMNS 80266, SMNS 84371, SMNS 84393; Figs. 4K-M) are well vascularized and fibrolamellar bone is locally deposited (Figs. 4K, L; Table 1). In *Ceresiosaurus*, parallel-fibred bone tissue is moderately vascularized (see also Hugi, 2011; Figs. 6J-M).

The periosteal bone of medium-sized Eosauropterygia is essentially made of parallel-fibred bone, whose vascular density and periosteal tissue organization is variable. However, vascular density is usually moderate. The bone tissue between the pachypleurosaur *Anarosaurus* (Figs. 4E, H) and *Nothosaurus* (Figs. 4F, I) differs mainly in its degree of tissue organization and vascular density. Tissue in *Nothosaurus* is less vascularized and more highly organized. In addition, *Anarosaurus* can display incompletely lined primary osteons and woven bone resulting in incipient fibrolamellar bone (Klein, 2010; Klein and Griebeler, 2018)

Locally, mainly in nothosaur ribs, the periosteal tissue is interspersed or even overprinted by different types of fibres. Sharpey's fibres, short angled, or longitudinal fibres can occur (Figs. 4N, O). Generally, the amount of fibres is the highest in distal samples but other parts of the rib can also contain fibres, most likely depending on the anatomical position of the rib.

The medullary region of ribs consists in all studied taxa of a matrix of calcified cartilage scattered with erosion cavities that are lined or filled by endosteal bone (Figs. 3, 5).

In some specimens, the medulla is lined by a sharp line with calcified cartilage along its inner margin (Figs. 5D, E, I- L). This sharp line separates the endochondral territory from the periosteal territory and is also described for sauropterygian long bones (Klein and Griebeler, 2016, 2018; Klein et al., 2016b). A sharp line is proximally visible in SMNS 84393, SMNS 80266, and SMNS 54434, medially in samples of SMNS 80266, SMNS 84393, SMNS 54434, Wijk09-557, *N. edwardsii*, and *Serpianosaurus*. It is visible in nearly all distal samples.

Resorption occurs only in the inner cortex of Wijk09-382 (Fig. 3E) and locally in the placodont rib. In the latter, only primary osteons are affected by resorption whereas in Wijk09-382 the entire periosteal cortex is affected. Beyond this exception, remodelling of periosteal bone was in no sample observed and was also not extensive in the medullar territory.

Gastralia

All studied gastralia (*Neusticosaurus*, *Serpianosaurus*, *Nothosaurus* spp., small Eosauropterygia indet.) share a thick periosteal cortex consisting of avascular lamellar bone. In most samples, the medullary territory is completely

filled by endosteal bone. In medial samples, growth marks resemble morphological shape changes from triangular to oval or round cross-section (Figs. 6N-P).

DISCUSSION

Comparison with other tetrapod vertebrae and ribs

Vertebrae

An overview of microanatomy in amniote vertebrae is given in Houssaye et al. (2016), revealing a high morphological and microanatomical variability. Amniote vertebrae generally display a spongious inner organization with two thin walls of compact bone at the periphery and around the neural canal (see Houssaye et al., 2014). The tightness of the vertebral trabecular network strongly varies among taxa (Dumont et al., 2013; Houssaye et al., 2014, 2016; Skutschas and Vitenko, 2017). Most semi-aquatic taxa (shallow swimmers to deep divers) show an inner organization similar to that of terrestrial taxa whereas exclusively aquatic taxa display either i) an increase in the tightness of the spongiosa (more numerous and proportionally thinner trabeculae with reduced intertrabecular spaces) and a reduction in thickness of the surrounding compact layers (active swimmers; Dumont et al., 2013; Houssaye et al., 2016; Skutschas and Vitenko, 2017), or ii) an increase in vertebral compactness, from a thickening of the compact cortical layers, like in sirenians (Hayashi et al., 2013), to an extreme thickening with almost completely

compact vertebrae, like in some Late Cretaceous marine squamates (see Houssaye, 2013). Such compact vertebrae were so far known only in some varanoid lizards, pythonomorphs, hind-limbed snakes, and in mesosaurs (NK pers. obs.) and to a lesser extent in the diapsid *Claudiosaurus* (Buffrénil and Mazin, 1989). Our study reveals that this extreme pachyosteosclerotic pattern also occurs in the pachypleurosaurs from the Alpine Triassic (*Neusticosaurus*, *Serpianosaurus*) where it is the result of an increase in cortical deposits and in inner bone compaction, strong inhibition of primary bone resorption, and the persistence of calcified cartilage (incomplete endochondral ossification). Conversely, there is a rather moderate osteosclerotic pattern in vertebrae of medium-sized eosauropterygians from Winterswijk locality, which is however, achieved by the same processes, except for the persistence of calcified cartilage at midshaft in the long bones. The placodont vertebra displays an increase in cortex thickness, which has however a spongious structure, due to a general high vascular density, local primary trabecular structure, and resorption of primary osteons. This contradicting signal (increase of periosteal thickness and increase of porosity) was also described for some placodont long bones (Klein et al., 2015b). Vertebrae of large *Nothosaurus* are not osteosclerotic due to the presence of large cavities in the neural arch and centrum, resulting in a cavernous structure.

The presence of large cavities in the core of vertebral centra involves complete reorganization and redistribution of the mass in the vertebrae and is in this extend unique among tetrapods (Dumont et al., 2013; Houssaye et al., 2014). Early Cretaceous choristoderes also show central cavities in the vertebral centrum but they are smaller (with one exception: see Skutschas

and Vitenko, 2017:fig.9J) as is the central cavity in a cervical vertebra of a Jurassic plesiosaur (Wintrich et al. 2017). The retainment of a notochordal canal can be interpreted as an adaptation to an aquatic lifestyle (paedomorphosis). However, such a cavity does not occur in vertebrae of the pachypleurosaur *Serpianosaurus*, were it is filled up with endosteal bone to achieve increase in bone mass. It is also not observed in the sacral vertebra (Wijk10-535), which might be related to its anatomical position, and is also not visible in SMNS 54418, which is most likely related to a non-central sampling location. In StIPB R68b the central cavity is also relatively small when compared to the condition in Eosauropterygia. Its shape is triangular, with two ventrally reaching legs, most likely representing nutrient foramina.

A further preliminary observation of our study reveals that dorsal centra of Eosauropterygia seem to be generally more compact than centra of cervical and sacral vertebrae (see Figs. 1B-F).

Ribs

Rib microanatomy was in the focus of a few studies (e.g., Amson et al., 2014; Buffrénil et al., 1990, 2010; Canoville et al., 2016; Houssaye et al., 2015) but comparison is often difficult due to the lack of a homologous sampling location along the ribs and between ribs along the ribcage (Houssaye et al., 2016). Canoville et al. (2016) were the first who provided an overview of rib inner organization conducted on a large sample of extant amniotes from which standardized midshaft sections of mid-dorsal ribs were taken. They found that ribs exhibit an ecological

signal. Thus, ribs of terrestrial taxa generally consist of a rather tubular structure with a peripheral compact cortical layer and either an open medullary cavity or an inner loose spongiosa. Amniotes inhabiting shallow waters globally show higher rib compactness than terrestrial relatives. To the contrary, flying amniotes generally possess relatively thinner cortices (Amson et al., 2014; Buffrénil et al., 1990, 2010; Canoville et al., 2016). However, some marine mammals (cetaceans) display a great variability in rib compactness, reaching from osteoporotic-like ribs to ribs with thick compact cortices, which is however, in some taxa, related to a variable habitat (Canoville et al., 2016; Houssaye et al., 2015). Microanatomical variability of the ribs is also high in mosasaurs (Houssaye and Bardet, 2012).

In spite of some variability, the rib microanatomy of Triassic sauropterygians is relatively uniform and generally results in osteosclerosis. The latter is achieved by the persistence of calcified cartilage and by an inhibition of remodeling. Although the proportions in the amount of periosteal and endosteal tissue change from the rib head towards the distal end of the rib, global compactness of the rib does not change significantly along the shaft. This is because incomplete endochondral ossification results in rather compact medullary regions (Figs. 3, 5; Table 1). The observed histological variability reflects differences in sampling location along the rib shaft as well as taxonomical differences and different anatomical positions and thus function of the ribs in the trunk region (e.g., presence of fibers). A correlation of the development of the spongiosa in the medullary region with size as Canoville et al. (2016) found, was not documented for Triassic Sauropterygia.

Surmik et al. (2018: figs. 2, 3) thin sectioned the proximal part of a pachyostotic dorsal rib from the Anisian of Poland that probably belongs to a pistosauroid. The Gogolin Formation, from which this specimen originates, also represents a near coastal, shallow marine environment. Besides differences in vascular system (dominance of small longitudinal ?simple vascular canals), the periosteal as well as the endosteal domains are significantly more compact than in any rib from our sample, including similar-sized nothosaur ribs. Differences are most likely related to taxonomy rather than to the anatomical position of the sampled element or the environment in which the animal lived. This again indicates the use of histology, at least in some groups, to distinguish taxa or support taxonomical assignment. An Upper Jurassic plesiosaur rib is, however, comparable in compactness (i.e., degree of osteosclerosis) and microanatomical organization along the shaft to our large nothosaur ribs (Street and O'Keefe, 2010).

Striking is the high amount of short fibers along the shaft in many of the rib samples, with a dominance in the medial to distal part of the rib and in general in large nothosaur samples (Table 1). In some samples, the entire periosteal tissue is overprinted by these short fibers (Figs. 4N, O). Sharpey's fibers, which are longer, seem to be restricted to the proximal part of the rib. The high amount of fibers in some dorsal ribs might be related to their anatomical position (i.e. anterior) and their possible association with thorax musculature and involvement into costal breathing (Carrier and Farmer, 2000; Perry and Sander, 2004). The placodont rib sections are completely free of any fibers, which is probably related to a different (i.e., more posterior)

anatomical position (i.e., functional signal related to breathing) although taxonomical differences can also not be excluded.

Gastralia

All studied gastralia of Eosauropterygia consist of avascular lamellar bone tissue and are pachyosteosclerotic. They lack any fibres, which might be related to their anatomical position. The Jurassic marine pleurosaurid *Paleopleurosaurus* shows a similar osteosclerotic gastralium (Klein and Scheyer, 2017) as do some ichthyosaurs (Kolb et al., 2011). Conversely, the gastralium of the Upper Jurassic plesiosaur (Street and O'Keefe, 2010) is pachyostotic but has a spongious inner structure. A gastralium of early Cretaceous choristoderes also exhibits compact avascular bone but has a small free medullary cavity (Skutschas and Vintenlo, 2017).

Comparison of sauropterygian ribs and vertebrae, with long bones

Placodontia indet.

The sampled placodont rib and vertebra have a comparable microstructure to that of the long bones of fast growing placodont taxa (Klein et al., 2015b, 2015c) (Table 2). They all share fibrolamellar bone tissue type and a high vascular density. Primary osteons are arranged radially or longitudinally in circumferential rows. A primary mainly radial trabecular structure can locally occur. They also have in common that primary osteons are enlarged by resorption. Mainly longitudinal primary osteons are sheathed by lamellar bone but the canal is never filled up, which represents a special form of incomplete remodeling (Klein et al., 2015b). Conversely,

the thickness of the cortex is in these placodont bones increased by more deposits and an inhibition of resorption, resulting in clear osteosclerotic bones. However, high vascular density and resorption processes act towards the contrary: to bone mass decrease. Thus, bones of fast growing placodonts display a contradicting pattern of localized BMD and BMI in the same bones (Klein et al., 2015b, c).

Calcified cartilage is at midshaft of placodont long bones completely resorbed but persists in the medullary territory of ribs and vertebrae. The placodont rib shows a network of endosteal trabeculae enclosing calcified cartilage.

Considering bone tissue, vascular density, and organization, these placodonts have the highest growth rates among Triassic Sauropterygia, comparable to that of ichthyosaurs (Klein et al., 2015b), which have been sustained swimmers in the open sea (Houssaye et al., 2014). Placodonts however, are regarded as slow swimmers or bottom walkers (summarized in Klein et al., 2015b), independently of their armoured or unarmoured body plan. They are all durophageous, feeding on hard shelled, largely sessile invertebrates (Scheyer et al., 2011).

All samples of these fast growing placodonts show besides generally pachyostotic bones a similar osteosclerotic microanatomy (i.e. inner bone compaction that results in a small medullary cavity), independently of the environment in which they had been found: Some placodont samples originate from near coastal environments (rib from Winterswijk; long bones from Poland/Anisian) whereas others come from shallow marine environments (vertebra and long bones, Upper Muschelkalk of southern Germany/Ladinian). Beside a certain developmental

plasticity, the consistency in general histological and microanatomical characters over time (Anisian to Ladinian) is noticeable. It is not understood yet why some placodonts grew with fibrolamellar bone tissue types and others with lamellar zonal bone tissue types (Klein et al., 2015b).

Pachypleurosauria

Serpianosaurus and *Neusticosaurus* grew with uniform lamellar-zonal bone tissue type (Hugi et al., 2011; Klein and Griebeler, 2018; Sander, 1990; this study). Bone tissue is generally better organized (well organized parallel-fibered bone and lamellar bone) and less vascularized in *Serpianosaurus* than in *N. edwardsii*. The latter presents relatively higher vascular density, which is dominated by radial vascular canals and its tissue is dominated by less organized parallel-fibred bone. The persistence of high amounts of calcified cartilage is documented for long bones (at midshaft), vertebrae, and ribs in both taxa (Table 2). Thus, osteosclerosis (BMI) is in *Serpianosaurus* and *Neusticosaurus* mostly the result of an incomplete resorption of calcified cartilage and thus incomplete endochondral ossification. The retainment of calcified cartilage at midshaft of long bones distinguishes these taxa from other Sauropterygia, which do not show calcified cartilage at midshaft in long bones. Osteosclerosis is in these taxa always combined to an obvious pachyostosis (summarized in Rieppel, 2000). All studied bones of *Serpianosaurus* and *Neusticosaurus* (ribs, vertebrae and limb bones) are thus pachyosteosclerotic. Among

Triassic Sauropterygia, they show the most numerous adaptive features and highest degree to an aquatic lifestyle.

Considering organization of bone tissue, vascular pattern and density as well as the deposition of regular annual growth marks, these pachypleurosaurs have the lowest growth rates among all Triassic Sauropterygia (Klein and Griebeler, 2016, 2018). *Serpianosaurus* and *Neusticosaurus* are small animals (around 1 m) with an elongated body shape (long neck, trunk, and tail), and a small head. They are regarded as axial swimmers, hunting for invertebrates such as arthropods/decapods or small fishes (Rieppel, 2002). They lived in shallow marine to open sea habitats (Alpine Triassic; Röhl et al., 2001).

Anarosaurus heterodontus

Some of the rib samples are assigned to the pachypleurosaur *Anarosaurus heterodontus* on the basis of its characteristic bone tissue type (Table 1). Bone tissue type as well as microanatomical pattern of *Anarosaurus* differ largely from those of the pachypleurosaur *Dactylosaurus* as well as from pachypleurosaurs from the Alpine Triassic (*Serpianosaurus-Neusticosaurus* clade) (Hugi et al., 2011; Klein, 2010; Klein and Griebeler, 2018). Rib and long bones of *Anarosaurus* both display moderate osteosclerosis, achieved by an increase of cortical thickness through a reduction of the medullary cavity when compared to the ancestral terrestrial condition. *Anarosaurus* is only known from coastal to near coastal environments of Winterswijk and central Germany (Rieppel, 2000). *Anarosaurus* was clearly less adapted to an aquatic lifestyle than other

pachypleurosaurs regarding its microanatomy and morphology but had a much higher growth rate as shown by its incipient fibrolamellar bone tissue (Klein, 2010; Klein and Griebeler, 2018).

Nothosaurus spp.

Bone tissue type, vascularization pattern and density are consistent between long bones, ribs and vertebrae in nothosaurs (Klein, 2010; Klein et al., 2016b; this study). Nothosaur bones are dominated by parallel-fibred tissue that shows different degrees of organization (low to high) and includes even unusual parallel-fibred bone (Houssaye et al., 2013; Klein et al., 2016b). Sometimes woven bone is deposited as well, forming—in combination with primary osteons—locally fibrolamellar bone or incipient fibrolamellar bone when primary osteons are only incompletely lined up by endosteal lamellar bone (Klein, 2010). Vascularization is dominated by longitudinal and radial canals as in other Sauropterygia. Vascular density is in average moderate but can vary. Growth rate in nothosaurs is clearly higher than in modern reptiles and distinctly higher than in pachypleurosaurs from the Alpine Triassic but not as high as in the pachypleurosaur *Anarosaurus* or in fast growing placodonts (Klein, 2010; Klein and Griebeler, 2016, 2018; Klein et al., 2016b).

The microanatomical pattern in nothosaur long bones is however not as consistent as in other Sauropterygia (Table 2). Klein et al. (2016b) described five microanatomical categories for *Nothosaurus* spp. humeri, two of which are unique among amniotes. These categories range from extreme osteosclerotic to very thin-walled cortices and involve different processes (i.e. increase

in cortical thickness through a reduction of the medullary cavity; reduction of the cortex due to an enlargement of the medullary cavity, spongy resorption pattern of periosteal bone). The microanatomy of nothosaur ribs is uniform and osteosclerotic, independent if they belong to small or large bodied nothosaur taxa. Vertebrae of small nothosaurs show a moderate osteosclerosis but in large *Nothosaurus* the structure is cavernous (large cavities in the neural arch and centrum).

In the Anisian, nothosaurs were small to medium sized animals (1.5 m - 3 m), but some taxa became rather large during the Ladinian, reaching more than 6 m in body length (summarized in Rieppel and Wild, 1996 and Rieppel, 2000). They all share a dorsoventrally flattened, elongated body. According to Caroll and Gaskill (1985) the forelimbs were used for propulsion, the hindlimbs for manoeuvring, and the tail helped to the propulsion by undulating. Nothosaurs had a heterodont dentition, including large fangs that suggest piscivory, although stomach contents also include small-bodied marine reptiles (Rieppel, 2002). Small-bodied nothosaurs (*Nothosaurus marchicus*) are known from Anisian near coastal to coastal environments (Winterswijk and Poland) whereas large bodied nothosaurs inhabited shallow marine and open marine environments but some forms may have stayed near coasts as well (Upper Muschelkalk; Klein et al. 2016b). Environmental differences and habitat preferences of individuals might be the main cause for microanatomical diversity as is observed in some modern marine mammals. However, taxonomic differences and developmental plasticity must be

considered, too. Additionally, it could well be that some large nothosaurs would exhibit osteosclerotic vertebrae but that they have simply not been sampled yet (sampling bias).

The rib Wijk07-31 shows a very highly organized avascular bone tissue, which does not evoke that of *Nothosaurus marchicus* or *Anarosaurus*. Size and high tissue organization might fit to bone tissue of *Lariosaurus* (Hugi, 2011), whereas the limited osteosclerosis does not fit to *Ceresiosaurus* (Hugi, 2011), the sister group of *Lariosaurus* (Rieppel; 2000). It also differs from the microanatomical patterns of *N. marchicus* and *Anarosaurus*.

Other marine reptiles

Other marine reptiles, such as the Permian *Claudiosaurus* (Buffrénil and Mazin, 1989) and *Mesosaurus* (NK pers. obs.), some Late Cretaceous marine squamates (Houssaye, 2013) also show strongly pachyosteosclerotic bones. However, they do not retain calcified cartilage in their medullary regions but rather achieved osteosclerosis through either intensive remodelling with excessive secondary bone deposits or through an inhibition of bone resorption, sometimes accompanied by an inhibition of calcified cartilage but only in the trabeculae of endochondral origin (see also Table 2).

CONCLUSIONS

The microanatomy and histology of studied long bones, ribs, and vertebrae are in general consistent within taxa. Except for some large *Nothosaurus* specimens, bones of Triassic Sauropterygia exhibit generally osteosclerosis and thus BMI. The pachypleurosaurs

Neusticosaurus and *Serpianosaurus* show the strongest osteosclerosis, coupled with pachyostosis. The pachypleurosaur *Anarosaurus* and *Nothosaurus marchicus* show moderate osteosclerosis. Placodonts also have pachyosteosclerotic bones due to the increase of cortex thickness but resorption of vascular spaces counteracts this on the histological level. In large *Nothosaurus* osteosclerosis is lowest or in some even not present, respectively.

We identified three main processes in how osteosclerosis is achieved in Triassic sauropterygians: 1) In the pachypleurosaurs *Neusticosaurus* and *Serpianosaurus* osteosclerosis is in all bones (ribs, vertebrae, and long bones) the result of incomplete endochondral ossification, i.e. the persistence of high amounts of calcified cartilage. 2) In long bones of fast growing placodonts and of some large *Nothosaurus*, osteosclerosis is the result of a strong increase in cortical thickness through a reduction of the medullary cavity and an inhibition of bone resorption. Calcified cartilage can also occur but is only limited. 3) In the placodont rib and vertebra some calcified cartilage is retained but also not in the same amount as in *Neusticosaurus* and *Serpianosaurus*. The pachypleurosaur *Anarosaurus* and the small nothosaur *Nothosaurus marchicus* show a similar pattern: no calcified cartilage at the midshaft of long bones but in the ribs and vertebrae. Both taxa achieve osteosclerosis by a moderate increase in cortical thickness through the reduction of the medullary cavity and by an inhibition of remodeling. All large nothosaur ribs are osteosclerotic; they retain some calcified cartilage and show an increase in cortical thickness, whereas the vertebrae of large nothosaurs are cavernous.

All gastralia are osteosclerotic with a thick avascular cortex, and the lack of a medullary cavity in most cases.

All sauropterygians share an inhibition of remodeling (see also Klein et al. 2015b,c, 2016b). Some resorption may occur (mainly in the placodont and some large nothosaur bones) but redeposition of bone does not occur at all or is incomplete. The processes leading to osteosclerosis in Sauropterygia are different to that observed in diapsid marine reptiles form the Permian (i.e. *Claudiosaurus*, Buffrénil and Mazin, 1989; *Mesosaurus*, Ricqlès, 1976; NK pers. obs.) where an imbalanced remodeling with excessive secondary bone deposits leads to osteosclerosis. Ichthyosaurs differ in general due to the occurrence of a secondarily compacted spongiosa near the growth center in long bones conferring BMI in this region, whereas the rest of the bone organization remains spongious and rather evokes BMD (Houssaye et al., 2014). Mosasaurs tendentially show BMD, except for the humerus of *Dallasaurus* (Houssaye et al., 2013).

However, the results of our work can only be preliminary because of taxonomical uncertainties, and due to small sample size, variations along the vertebral column and the rib cage cannot be addressed adequately.

ACKNOWLEDGMENTS

We are grateful to E. Maxwell, R. Schoch (both SMNS), M. Sander (StIPB), and T. Scheyer (PIMUZ) for the permission to sample specimens or use existing samples under their care.

Ch. Wimmer-Pfeil (SMNS) and O. Dülfer (StIPB) are acknowledged for the production of thin sections. We also would like to thank P. Skutschas (SPBU), D. Surmik (WNOZ), as well as an anonymous reviewer for their helpful comments and suggestions.

REFERENCES

Amson E, de Muizon C, Laurin M, Argot C, Buffrénil V de. 2014. Gradual adaptation of bone structure to aquatic lifestyle in extinct sloths from Peru. Proc Roy Soc London S B Biol Sc 281:20140192.

Amson E, Billet G, Muizon C de. 2018. Evolutionary adaptation to aquatic lifestyle in extinct sloths can lead to systemic alteration of bone structure. Proc R Soc B 285:20180270.

Buffrénil V de, Mazin JM. 1989. Bone histology of *Claudiosaurus germaini* (Reptilia, Claudiosauridae), and the problem of pachyostosis in aquatic tetrapods. Hist Biol 2:311-322.

Buffrénil V de, Mazin JM. 1990. Bone histology of the ichthyosaurs: comparative data and functional interpretation. Paleobiol 16:435-447.

Buffrénil V de, Sire JY, Schoevaert D. 1986. Comparaison de la structure et du volume squelettiques entre un delphinidé (*Delphinus delphis* L.) et un mammifère terrestre (*Panthera leo* L.). Can J Zool 64:1750-1756.

Buffrénil V de, Mazin JM, Ricqlès A de. 1987. Caractères structuraux et mode de croissance du fémur d'*Omphalosaurus nisseri*, ichthyosaurien du Trias moyen du Spitzberg. Ann Palaontol 73:195-216.

Buffrénil V de, Ricqlès A de, Ray CE, Domning DP. 1990. Bone histology of the ribs of the archaeocetes (Mammalia: Cetacea). J Vert Paleontol 10:455-466.

Buffrénil V de, Houssaye A, Böhme W. 2008. Bone vascular supply in monitor lizards (Squamata: Varanidae): influence of size, growth, and phylogeny. J Morphol 269:533-543.

Buffrénil V de, Canoville A, D'Anastasio R, Domning DP. 2010. Evolution of sirenian pachyosteosclerosis, a model-case for the study of bone structure in aquatic tetrapods. J Mammal Evol 17(2):101-120.

Carroll RL, Gaskill P. 1985. The nothosaur *Pachypleurosaurus* and the origin of plesiosaurs. Phil Trans R Soc Lond B 309(1139):343-93.

Canoville A, Laurin M. 2009. Microanatomical diversity of the humerus and lifestyle in lissamphibians. Acta Zool 90:110-122.

Canoville A, Laurin M. 2010. Evolution of humeral microanatomy and lifestyle in amniotes, and some comments on palaeobiological inferences. Biol J Linn Soc 100(2):384-406.

Canoville A, Buffrénil V de, Laurin M. 2016. Microanatomical diversity of amniote ribs: an exploratory quantitative study. Biol J Linn Soc 118(4):703-733.

Carrier DR, Farmer CG. 2000. The integration of ventilation and locomotion in archosaurs. Integr Comp Biol 40(1):87-100.

Dewaele L, Peredo CM, Meyvisch P, Louwye S. 2018 Diversity of late Neogene Monachinae (Carnivora, Phocidae) from the North Atlantic, with the description of two new species. R Soc Open Sci 5:172437.

Dumont M, Laurin M, Jacques F, Pellé E, Dabin W, Buffrénil V de. 2013. Inner architecture of vertebral centra in terrestrial and aquatic mammals: a two-dimensional comparative study. J Morphol 274:570-584.

Francillon-Vieillot H, Buffrénil V de, Castanet J, Géraudie J, Meunier FJ, Sire, Zylberberg L, Ricqlès A de. 1990. Microstructure and mineralization of vertebrate skeletal tissues. In: Carter JG, editor. Skeletal Biomineralization: Patterns, Processes and Evolutionary Trends. Vol. 1. New York: Van Nostrand Reinhold; 1990. p. 471-530.

Germain D, Laurin M. 2005. Microanatomy of the radius and lifestyle in amniotes (Vertebrata, Tetrapoda). Zool Scripta 34:335-350.

Gray N-M, Kainec K, Madar S, Tomko L, Wolfe S. Sink or swim? Bone density as a mechanism for buoyancy control in early cetaceans. Anat Rec 290:638-53.

Hayashi S, Houssaye A, Nakajima Y, Chiba K, Ando T, Sawamura H, Inuzuka N, Kaneko N, Osaki T. 2013. Bone inner structure suggests increasing aquatic adaptations in Desmostylia (Mammalia, Afrotheria). PLoS ONE 8(4):e59146.

Houssaye A. 2008. A preliminary report on the evolution of the vertebral microanatomy within mosasauroids (Reptilia, Squamata). In: Everhart M.J., editor. Proceedings of the Second Mosasaur Meeting. Fort Hays State University, Hays, Kansas. p. 81-89.

Houssaye A. 2009. “Pachyostosis" in aquatic amniotes: a review. Integr Zool 4(4):325-340.

Houssaye A. 2013. Palaeoecological and morphofunctional interpretation of bone mass increase: an example in Late Cretaceous shallow marine squamates. Biol Rev 88:117-139.

Houssaye A, Bardet N. 2012. Rib and vertebral micro-anatomical characteristics of hydropelvic mosasauroids. Lethaia 45:200-209.

Houssaye A, Mazurier A, Herrel A, Volpato V, Tafforeau P, Boistel R, Buffrénil V de. 2010. Vertebral microanatomy in squamates: structure, growth and ecological correlates. J Anat 217:715-727.

Houssaye A, Lindgren J, Pellegrini R, Lee AH, Germain D, Polcyn MJ. 2013. Microanatomical and histological features in the long bones of mosasaurine mosasaurs (Reptilia, Squamata)–implications for aquatic adaptation and growth rates. PLoS ONE 8(10): e76741.

Houssaye A, Scheyer TM, Kolb C, Fischer V, Sander PM. 2014. A new look at ichthyosaur long bone microanatomy and histology: Implications for their adaptation to an aquatic life. PLoS ONE 9(4): e95637.

Houssaye A, Waskow K, Hayashi S, Cornette R, Lee AH, Hutchinson J. 2015. Biomechanical evolution of solid bones in large animals: a microanatomical investigation. Biol J Linn Soc 2015:doi:10.1111/bij.12660.

Houssaye A, Fish FE. 2016. Functional (secondary) adaptation to an aquatic life in vertebrates: an introduction to the symposium. Integr Comp Biol 56:1266-1270.

Houssaye A, Sander PM, Klein N. 2016. Adaptive patterns in aquatic amniote bone microanatomy – More complex than previously thought. Integr Comp Biol 56:1349-1369.

Hugi J. 2011. The long bone histology of *Ceresiosaurus* (Sauropterygia, Reptilia) in comparison to other eosauropterygians from the Middle Triassic of Monte San Giorgio (Switzerland/Italy). Swiss J Palaeontol 130(2):297-306.

Hugi J, Scheyer TM, Sander PM, Klein N, Sánchez-Villagra MR. 2011. Long bone microstructure gives new insights into the life of pachypleurosaurids from the Middle Triassic of Monte San Giorgio, Switzerland/ Italy. C R Palevol 10(5–6):413-426.

Klein N. 2010. Long bone histology of Sauropterygia from the Lower Muschelkalk of the Germanic Basin provides unexpected implications for phylogeny. PLoS ONE 2010:5(7).

Klein N, Sander PM. 2007. Bone histology and growth of the prosauropod dinosaur *Plateosaurus* from the Norian bonebeds of Trossingen (Germany) and Frick (Switzerland). Spec papers Paleontol 77:169-206.

Klein N, Griebeler EM. 2016. Bone histology, microanatomy, and growth of the nothosauroid *Simosaurus gaillardoti* (Sauropterygia) from the Upper Muschelkalk of southern Germany/Baden-Württemberg. C R Palevol. 15(1–2):142-162.

Klein N, Scheyer TM. 2017. Microanatomy and life history in *Palaeopleurosaurus* (Rhynchocephalia: Pleurosauridae) from the Early Jurassic of Germany. Science Nat 104:4.doi:10.1007/s00114-016-1427-3.

Klein N, Griebeler EM. 2018. Growth patterns, sexual dimorphism, and maturation modeled in Pachypleurosauria from Middle Triassic of central Europe (Diapsida: Sauropterygia). Fossil Rec 21:137-157.

Klein N, Voeten DFAE, Lankamp J, Bleeker R, Sichelschmidt OJ, Liebrand M, Nieweg DC, Sander PM. 2015a. Postcranial material of *Nothosaurus marchicus* from the Lower Muschelkalk (Anisian) of Winterswijk, The Netherlands, with remarks on swimming styles and taphonomy. Pal Z 89(4):961-981.

Klein N, Houssaye A, Neenan JM, Scheyer TM. 2015b. Long bone histology and microanatomy of Placodontia (Diapsida: Sauropterygia). Contributions Zool 84(1):59-84.

Klein N, Neenan JM, Scheyer TM, Griebeler E-M. 2015c. Growth patterns and life history strategies in Placodontia (Diapsida: Sauropterygia). Royal Soc Open Sci 2:140440:doi: 10.1098/rsos.140440.

Klein N, Voeten DFAE, Haarhuis A, Bleeker R. 2016a. The earliest record of the genus *Lariosaurus* from the early middle Anisian (Middle Triassic) of the Germanic Basin. J Vert Paleontol 36(4):doi:10.1080/02724634.2016.1163712.

Klein N, Sander PM, Krahl A, Scheyer TM, Houssaye A. 2016b. Diverse aquatic adaptations in *Nothosaurus* spp. (Sauropterygia) –Inferences from humeral histology and microanatomy, PLoS ONE 11:e0158448.

Kolb C, Sánchez-Villagra MR, Scheyer TM. 2011. The palaeohistology of the basal ichthyosaur *Mixosaurus* (Ichthyopterygia, Mixosauridae) from the Middle Triassic: Palaeobiological implications. C R Palevol 10:403-411.

Krahl A, Klein N, Sander PM. 2013. Evolutionary implications of the divergent long bone histologies of *Nothosaurus* and *Pistosaurus* (Sauropterygia, Triassic). BMC Evol Biol 13:1-23.

Ksepka DT, Werning S, Sclafani M, Boles MZ. 2015. Bone histology in extant and fossil penguins (Aves: Spheniscifformes). J Anat 227(5):611-630.

Laurin M, Girondot M, Loth MM. 2004. The evolution of long bone microstructure and lifestyle in lissamphibians. Paleobiol 30:589-613.

Laurin M, Meunier F, Germain D, Lemoinei M. 2007. A microanatomical and histological study of the paired fin skeleton of the Devonian sarcopterygian *Eusthenopteron foordi*. J Paleontol 81:143-153.

Laurin M, Canoville A, Germain D. 2011. Bone microanatomy and lifestyle: a descriptive approach. C R Palevol 10(5-6):381-402.

Meyer Hv. 1847–1855. Die Saurier des Muschelkalks mit Rücksicht auf die Saurier aus Buntem Sandstein und Keuper. Zur Fauna der Vorwelt, 2te Abt, Frankfurt: Heinrich Keller; p. VIII+ 167.

Motani R. 2009. The evolution of marine reptiles. Evol: Educ Outreach 2:224-235.

Perry SF, Sander PM. 2004. Reconstructing the evolution of the respiratory apparatus in tetrapods. Respir Physiol Neurobiol 144:125-139.

Quémeneur S, Buffrénil V de, Laurin M. 2013. Microanatomy of the amniote femur and inference of lifestyle in limbed vertebrates. Biol J Linn Soc 109:644-655.

Ricqlès A de, Buffrénil V de. 2001. Bone histology, heterochronies and the return of tetrapods to life in water: where are we? In: Mazin JM, Buffrénil V de, editors. Secondary Adaptations of Tetrapods to Life in Water. München: Verlag Dr. Friedrich Pfeil. p. 289-310.

Rieppel, O. 1989. A new pachypleurosaur (Reptilia: Sauropterygia) from the Middle Triassic of Monte San Giorgio, Switzerland, Phil Trans R Soc Lond B 323:1-73.

Rieppel O, Wild R. 1996. A revision of the genus *Nothosaurus* (Reptilia: Sauropterygia) from the Germanic Triassic, with comments on the status of *Conchiosaurus clavatus.* Fieldiana Geol NS 34:1-82.

Rieppel O. 2000. Sauropterygia I—Placodontia, Pachypleurosauria, Nothosauroidea, Pistosauroidea. In: Wellnhofer P editor. Handbuch der Paläoherpetologie. München Verlag Dr. Friedrich Pfeil. 12A: p 1-134.

Rieppel O. 2002. Feeding mechanics in Triassic stem-group sauropterygians: the anatomy of a successful invasion of Mesozoic seas. Zool J Linn Soc 135(1):33-63.

Röhl H-J, Schmid-Röhl A, Furrer H, Frimmel A, Oschmann W, Schwark L. 2001. Microfacies, geochemistry and palaeoecology of the Middle Triassic Grenzbitumenzone from Monte San Giorgio (Canton Ticino, Switzerland). Geol Insubrica 6:1-13.

Sander PM. 1989. The pachypleurosaurids (Reptilia: Nothosauria) from the Middle Triassic of Monte San Giorgio (Switzerland) with the description of a new species. Philos T Roy Soc B 325:561-666.

Sander PM. 1990. Skeletochronology in the small Triassic reptile *Neusticosaurus*. Ann Sci Nat (Paris) 11:213-217.

Sander PM, Klein N, Albers PCH, Bickelmann C, Winkelhorst H. 2014. Postcranial morphology of a basal Pistosauroidae (Sauropterygia) from the Lower Muschelkalk of Winterswijk, The Netherlands. Pal Z 88:55-71.

Scheyer TM, Neenan JM, Renesto S, Saller F, Hagdorn H, Furrer H, Rieppel O, Tintori A. 2012. Revised paleoecology of placodonts—with a comment on 'The shallow marine placodont *Cyamodus* of the central European Germanic Basin: its evolution, paleobiogeography and paleoecology' by C.G. Diedrich. (Hist Biol 2011:1-19). Hist Biol 24(3):257-267.

Schröder H. 1914. Wirbeltiere der Rüdersdorfer Trias. Abh Königl Preuss Geol L-anstalt NF 65:1-98.

Skutschas PP, Vitenko DD. 2017. Early Cretaceous choristoderes (Diapsida, Choristodera) from Siberia, Russia. Cretac Res 77:79-92.

Street HP, O'Keefe SR. 2010. Evidence of Pachyostosis in the Cryptocleidoid Plesiosaur *Tatenectes laramiensis* from the Sundance Formation of Wyoming. J Vertebr Paleontol 30(4):1279-1282.

Surmik D, Szczygielski T, Janiszewska K, Rothschild BM. 2018. Tuberculosis-like respiratory infection in 245-million-year-old marine reptile suggested by bone pathologies. R Soc Open Sci 5:180225:doi.org/10.1098/rsos.180225.

Thewissen JGM, Nummela S. 2008. Sensory Evolution on the Threshold. Adaptations in Secondarily Aquatic Vertebrates. 1st ed. Berkeley, California: University of California Press.

Wintrich T, Scaal M, Sander PM. 2017. Foramina in plesiosaur cervical centra indicate a specialized vascular system. F R 20(2):279-290.

FIGURE LEGENDS

Figure 1

Microanatomical overview of sauropterygian vertebrae.

A, Composite microscopic pictures of longitudinal section of dorsal centrum Wijk08-47, Eosauropterygia, depicting compact periosteal cones and less compact endochondral cones.

B, Transverse section of complete cervical vertebra Wijk13-88, Eosauropterygia, depicting compact periosteal bone in the dorsal-lateral part of the neural arch and in the mediodorsal and ventral part of the centrum.

C, Transverse section of complete sacral vertebra Wijk10-535, Eosauropterygia, depicting compact periosteal bone only in the medio-lateral dorsal part of the neural arch and as a thin layer along the periphery of the centrum. The centrum does not have a free cavity but is spongious containing secondary trabeculae.
D, Transverse section of dorsal centrum Wijk08-94, Eosauropterygia, depicting thick compact bone along the latero-ventral periphery and dorsally in form of a thin vertical stripe.
E, Transversal section of dorsal centrum Wijk08-126, Eosauropterygia, in polarized light to visualize the distribution of periosteal and endochondral bone.
F, Transverse natural cut through a complete dorsal vertebra SMNS 54418, *Nothosaurus* sp., depicting a large central spongiosa made of small trabeculae surrounded by a regular thick layer of compact bone in the centrum.
G, Transverse section of dorsal centrum PIMUZ T 1568, *Serpianosaurus*, which is in general extremely compact.
H and I, Transverse section of dorsal centra PIMUZ T phz 161 and PIMUZ T 4757, *Neusticosaurus edwardsii*, which are less compact than those of *Serpianosaurus* due to strong radial vascularization, resulting in a general higher vascular density.
J, Transverse section of incomplete dorsal vertebra (StIPB R68a, *Nothosaurus* sp.). The centrum has a large free cavity and the lateral parts of the neural arch also display free cavities lined by thin layers of compact bone.
K, Transverse section of incomplete dorsal vertebra StIPB R68b, Placodontia indet. aff. *Cyamodus*, depicting compact periosteal bone in the ventrolateral centrum as well as a thick layer along the periphery of the preserved neural arch.

Figure 2
Vertebrae histology of Sauropterygia

A, Well-vascularized fibro-lamellar bone in the ventral part of the centrum of dorsal vertebra StIPB R68b (Placodontia indet. aff. *?Cyamodus*) in normal light. Note the resorption at the left side of the figure.

B, Well-vascularized fibro-lamellar bone in the lateral part of the centrum of dorsal vertebra StIPB R68b (Placodontia indet. aff. *?Cyamodus*) in normal light. Note the sheathed longitudinal primary osteons.

C, Detail of primary trabeculae in the centrum of dorsal vertebra StIPB R68b (Placodontia indet. aff. *Cyamodus*) in polarized light.

D, Compact periosteal bone in the ventrolateral part of the centrum Wijk08-111 (aff. *Nothosaurus*) in normal light depicting parallel-fibred bone tissue. The free cavity shows at its margin secondary trabeculae. Towards the outer margin tissue organization increases, vascularization decreases, and some growth marks are deposited.

E, Parallel-fibred bone with simple radial vascular canals in Wijk10-535 (aff. *Nothosaurus*) in polarized light.

F, Parallel-fibred bone with incompletely lined radial and longitudinal vascular canals in Wijk08-99 (aff. *Nothosaurus*) in polarized light.

G, Compact periosteal bone in the ventrolateral part of the centrum Wijk08-99 (aff. *Nothosaurus*) in normal light depicting detail of parallel-fibred bone tissue. In the upper half is untypical parallel-fibred bone tissue interspersed with a high number of large osteocytes visible. In the lower half is normal parallel-fibred tissue visible.

H, The same sample in polarized light.

I, Compact periosteal bone in dorsal vertebra StIPB R68a (large *Nothosaurus* sp.) in polarized light depicting parallel-fibred bone tissue with simple longitudinal vascular canals and some primary osteons.

J, Periosteal bone in dorsal vertebra StIPB R52 (large *Nothosaurus* sp.) in polarized light depicting parallel-fibred bone tissue with radially organized simple vascular canals. Note the funnel-shaped arrangement of tissue along the canals, typical for nothosaurs.

K, Transition between periosteal bone (upper left half) and endochondral bone (right lower half) in cervical vertebrae Wijk13-88 (Eosauropterygia) in polarized light.
L, Endochondral bone essentially made of calcified cartilage with some intertrabecular spaces lined by endosteal bone in dorsal centrum Wijk08-94 (Eosauropterygia).
M, Endochondral bone essentially made of calcified cartilage with some intertrabecular spaces lined by endosteal bone in dorsal centrum Wijk08-94 (Eosauropterygia).
N, Detail of endochondral bone consisting of calcified cartilage enclosed in endosteal trabeculae in StIPB R 68b (Placodontia indet. aff. *?Cyamodus*). The same endochondral tissue occurs in large *Nothosaurus* sp..
O, Suture between centrum and neural arch made of uncalcified cartilage in large Nothosaurus sp. (StIPB R 68a).
P, Endochondral region in the upper left half and periosteal bone in the lower right half in vertebra Wijk08-94 in polarized light.

Figure 3

Overview of sauropterygian rib microanatomy. Serial cross-sections of dorsal ribs sampled from the proximal (rib head) to the distal end, as shown in A (in normal light).
A1-4, Composite microscopic pictures of placodont rib Wijk16-GG.
B1-8, Rib Wijk07-31 (Eosauropterygia).
C1-3, Composite microscopic pictures of rib SMNS 54434 (Eosauropterygia) in normal light.
D1-6, Composite microscopic pictures of rib Wijk09-557 (Eosauropterygia) in normal light except for D-2 which is in polarized light.
E1-4, Composite microscopic pictures of rib Wijk09-382 (Eosauropterygia) in normal light.
F1-3, Composite microscopic pictures of rib SMNS 84393 (*Nothosaurus* sp.) in normal light.
G1-4, Composite microscopic pictures of rib SMNS 80266 (*Nothosaurus* sp.) in normal light.

Figure 4

Various periosteal tissue types observed in proximal samples of sauropterygian ribs.

A, Periosteal and endosteal domain in the placodont rib Wijk16-GG in normal light. Note the resorption of the cortex.

B, Fibrolamellar bone in the placodont rib in normal light and

C, Detail of bone tissue in the placodont rib in polarized light.

D, Highly organized avascular parallel fibred bone tissue in Eosauropterygia Wijk07-31in normal light.

E, Poorly organized parallel-fibred bone and local incipient fibrolamellar bone in the inner cortex and highly organized parallel fibred tissue in the outer cortex in the pachypleurosaur ?*Anarosaurus* Wijk09-37 in normal light.

F, Parallel-fibred bone tissue in ?*Nothosaurus marchicus* Wijk09-382 in normal light.

G, Same sample as in D-F (Eosauropterygia Wijk07-31) in polarized light.

H, Low organized parallel-fibred tissue and local incipient fibrolamellar bone in the inner cortex and higher organized parallel fibred tissue in the outer cortex in a rib of the pachypleurosaur ?*Anarosaurus* Wijk09-37 in polarized light.

I, Parallel-fibred bone tissue in ?*Nothosaurus marchicus* (Wijk09-382) in polarized light (same samples as in F).

J, Parallel-fibred bone with mainly longitudinal vascular canals in ?*Nothosaurus* SMNS 54434 in normal light.

K, Parallel-fibred bone with mainly longitudinal simple vascular canals and some primary osteons in large *Nothosaurus* sp. SMNS 96929-6 in normal light.

L, Parallel-fibred bone tissue with mainly radial vascular canals and some primary osteons in large *Nothosaurus* sp. SMNS 80266 in polarized light.

M, Unusual parallel-fibred bone tissue in large *Nothosaurus* sp. SMNS 96929-6 in polarized light.

N, Detail of bone tissue overprinted by fibers in large *Nothosaurus* sp. SWMNS 80266.

O, Periosteal bone in medial sample of large *Nothosaurus* sp. SMNS 80266 depicting resorption (erosion cavities) and the periosteal tissue largely replaced by fibers in polarized light.

Figure 5.

Details of medullary regions and endosteal bone.

A, Medial sample of the placodont rib (Wijk16-GG) in normal and B, polarized light. Note the large medullary region largely filled by trabeculae that enclose calcified cartilage.

C, Detail of calcified cartilage in the placodont rib Wijk16-GG in normal (right side) and polarized (left side) light.

D, Detail of medullary cavity largely filled by endosteal bone and surrounded by a sharp line and calcified cartilage in proximal rib sample of Wijk10-130 (aff. *Anarosaurus*)

E, Detail of medullary region in the proximal rib of ?*Nothosaurus marchicus* (Wijk09-382) in polarized light. The cavity is here only partially filled by endosteal bone but also surrounded by a sharp line and calcified cartilage.

F, Transition between medullary cavity lined by a thin layer of endosteal bone and periosteal bone in proximal rib sample of large *Nothosaurus* (SMNS 96928) in normal light.

G, Medullary region consisting of large erosion cavities scattered into the periosteal bone in proximal rib sample of large *Nothosaurus* (SMNS 80266) in normal light.

H, Medullary region consisting of large erosion cavities lined by endosteal bone in medial rib sample of large *Nothosaurus* (SMNS 80266) in normal light.

I, Medullary region filled by calcified cartilage and erosion cavities lined by endosteal bone in medial sample of SMNS 54434 (Eosauropterygia) that is surrounded by a sharp line.

J, Cross section of the medial part of the rib of ?*Nothosaurus marchicus* (Wijk09-382) in polarized light. Note the already reduced cortex and the medullary region filled by calcified cartilage and endosteal bone.

K, Distal sample of large *Nothosaurus* (SMNS 81881) in polarized light. The medullary region is surrounded by a thin layer of periosteal cortex.

L, Distal sample of ?*Nothosaurus marchicus* (Wijk06-123) in polarized light. The entire section is made of the medullary region.

M, Detail of the transition from the enlarged medullary region (calcified cartilage, erosion cavities, and endosteal bone) and the reduced periosteal cortex in distal sample of Eosauropterygia indet. (Wijk07-31).

N, Detail of medullary region of distal rib sample of a ?*Nothosaurus marchicus* (Wijk06-123) in polarized light depicting calcified cartilage and large erosion cavities lined by endosteal bone in polarized light.

O, Detail of medullary region containing calcified cartilage and largely filled by endosteal bone in a large *Nothosaurus* (SMNS 96928) in polarized light.

Figure 6.

A-M, Rib cross sections of the pachypleurosaurs *Serpianosaurus* and *Neusticosaurus,* and of the nothosaur *Ceresiosaurus*, all from the Alpine Triassic. N-P, Osteosclerotic gastralia of Eosauropterygia. Samples are figured in normal light if not mentioned otherwise.

A-D, Samples of dorsal ribs of *Serpianosaurus*. A, Proximal part of a dorsal rib (PIMUZ T 1565). B, Proximal part of a dorsal rib PIMUZ T 1564). C, Medial part of a dorsal rib (PIMUZ T 131). D, Distal part of a dorsal rib (PIMUZ T 1564).

E-I, Samples of dorsal ribs of *Neusticosaurus edwardsii*. E, Proximal part of a dorsal rib (PIMUZ T 4757). F, Medial part of a dorsal rib (PIMUZ T phz 14). G, Medial part of a dorsal rib (PIMUZ T 4748). H, I, Distal part of a dorsal rib (PIMUZ T 4757) in normal and polarized light.

J-M, Samples of dorsal ribs of *Ceresiosaurus.* J, Rib head of a dorsal rib (PIMUZ T phz 296). K, Proximal part of a dorsal rib (PIMUZ T 5622). L, Medial part of a dorsal rib (PIMUZ T 5622). M, Distal part of a dorsal rib (PIMUZ T 5153).

N1-2, Proximal and medial cross section of a gastralium (SMNS 54413).

O1-2, Proximal and medial cross section of a gastralium (Wijk09-27).

P, Cross section of a large gastral rib of *Nothosaurus* (SMNS 81882).

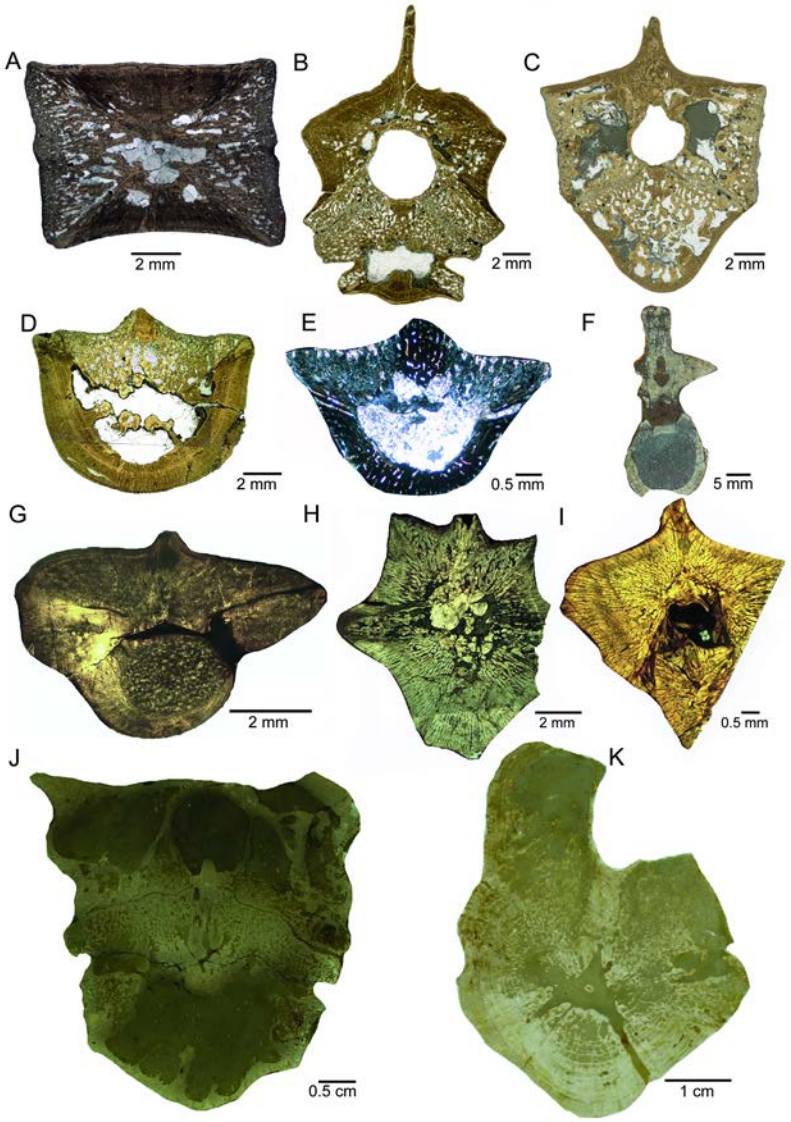

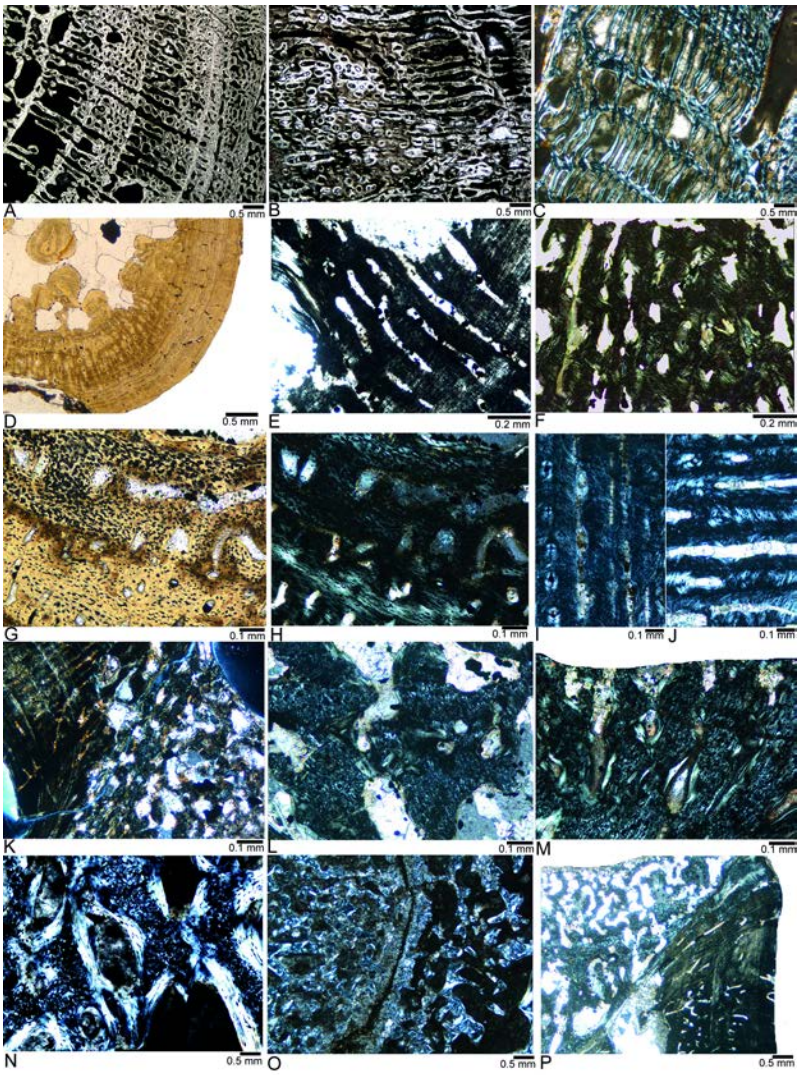

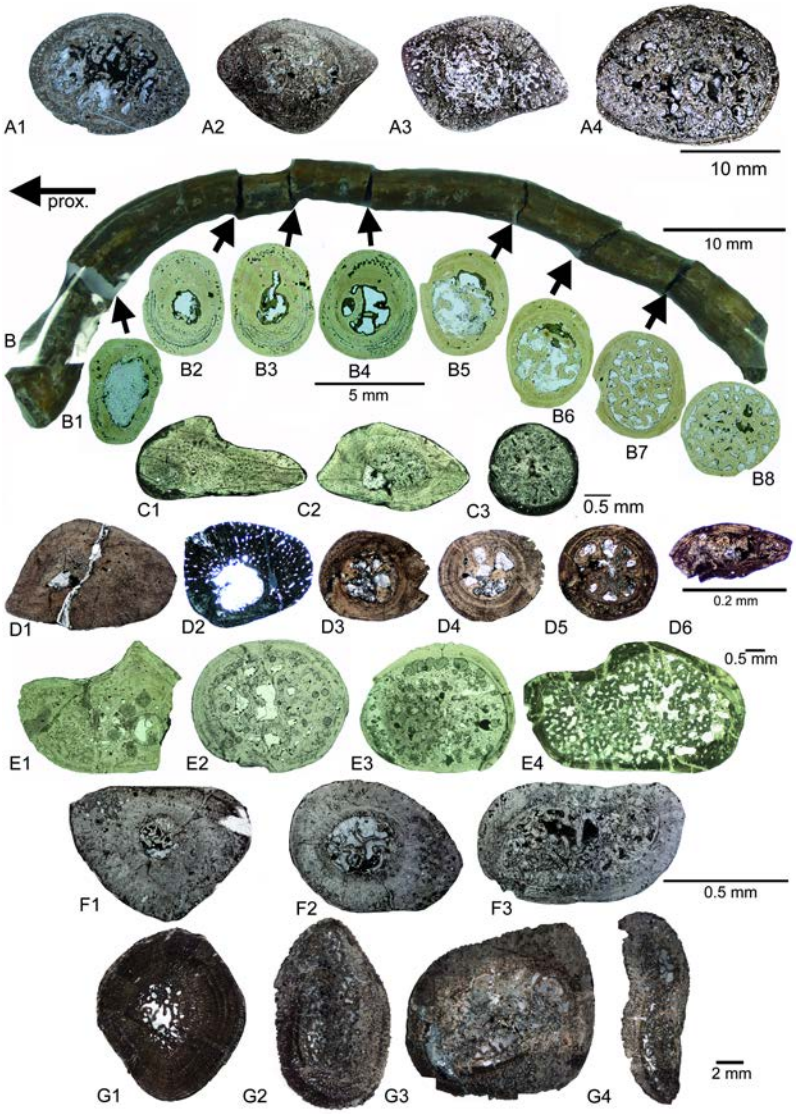

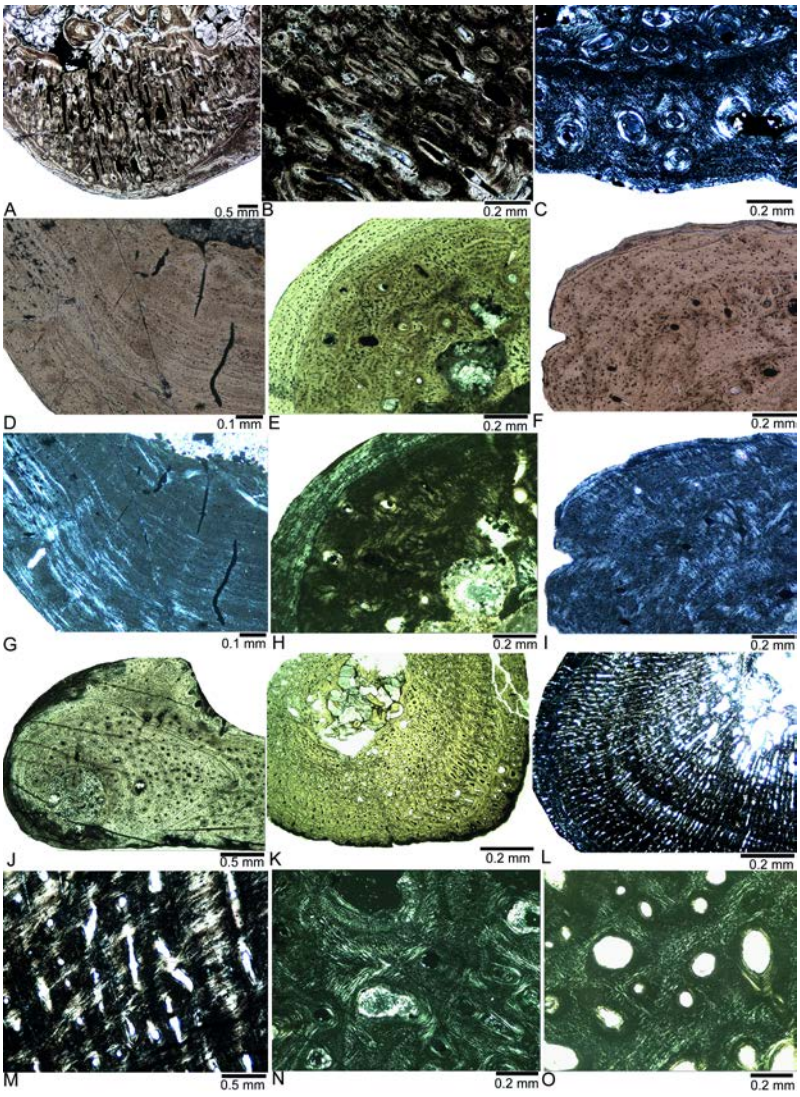

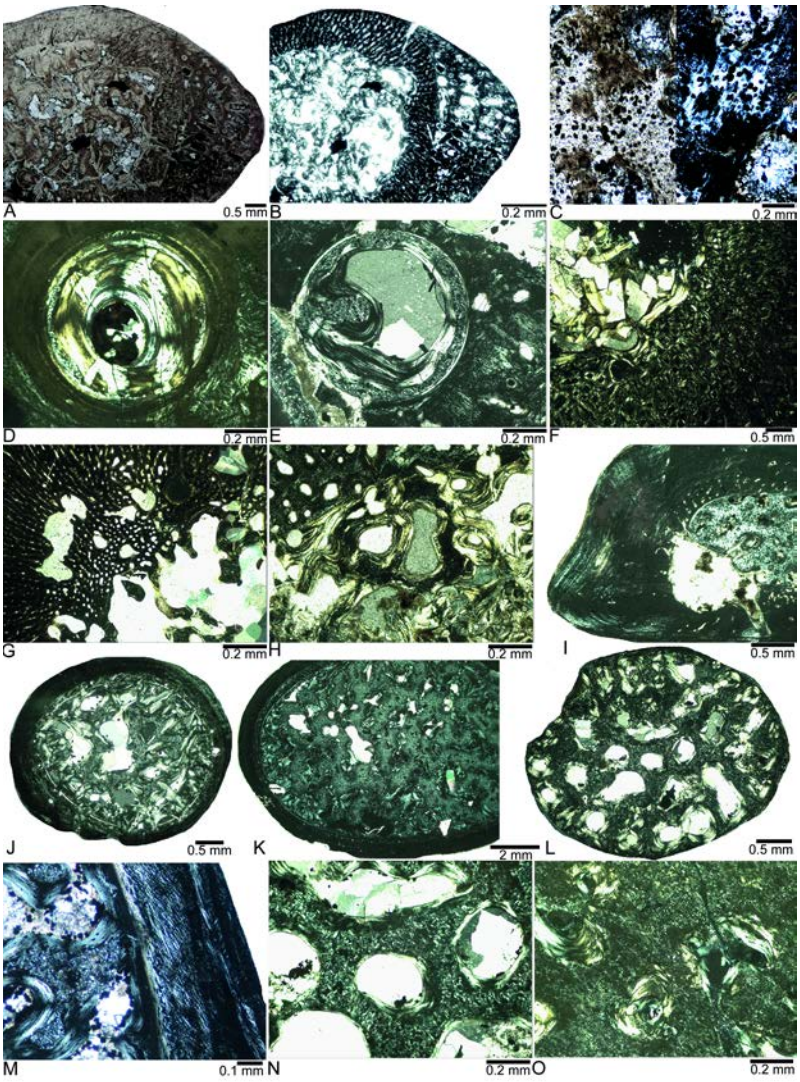

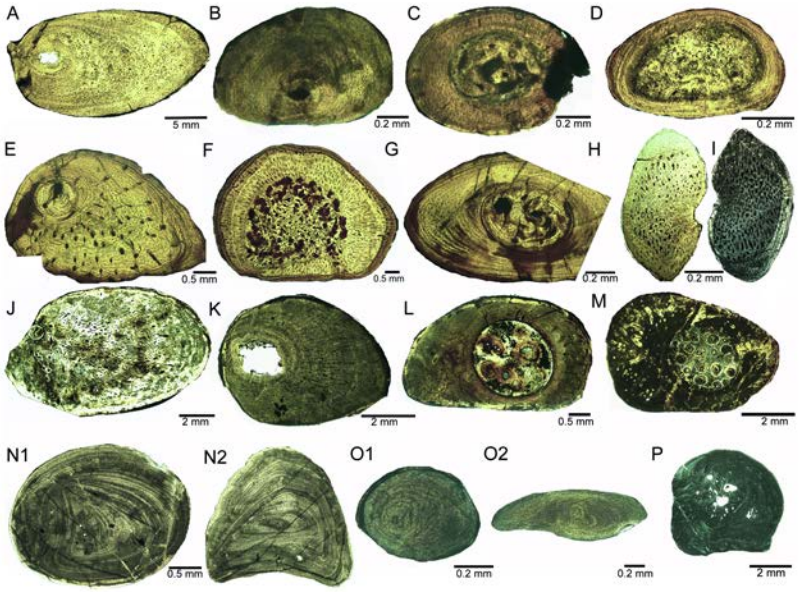

Table 1. Stratigraphic age, locality information, and measurements as well as histological and microanatomical information of sampled ribs and vertebrae. Abbreviations: Lb, lamellar bone; pfb, parallel-fibred bone; FLB, fibrolamellar bone tissue po, primary osteons; svc, simple vascular canals;

Repository number/ anatomical position	**locality & age**	**height x width (cm)**	**microanatomy**	**histology**	**taxonomical assignment**
Vertebrae					
Placodontia					
StIPB R 68b incomplete dorsal	Bayreuth early Ladinian	>5.65 x 4.35	osteosclerosis; thick compact cortex but spongious by vascular system; triangular small centrum cavity; spongious facet tissue	FLB with high radial vascular density (incl. primary trabeculae); resorption of primary osteons	?*Cyamodus*
Nothosauridae					
StIPB R 52 dorsal centrum	Bayreuth early Ladinian	2.85 x ~4.2	large centrum cavity surrounded by a thin layer of compact bone; spongious facet tissue	mainly pfb, locally incipient FLB; radially svc, incompletely and completely lined po	*Nothosaurus* sp.
StIPB R 68a incomplete ?sacral	Bayreuth early Ladinian	>4.55 x 4.3	cavernous neural arch; spongious facet tissue; large centrum cavity, surrounded by a thin layer of compact bone	mainly pfb, locally incipient FLB; radially svc, incompletely and completely lined po	*Nothosaurus* sp.
SMNS 54418 complete dorsal	Gogolin/Poland Bithnyian	3.7 x ~2.0	compact neural arch with a central cavity; large spongious medullary region (nearly empty cavity) surrounded by a thin layer of compact bone	no thin section available	*Nothosaurus* sp.
Wijk13-88 complete cervical	Winterswijk Anisian	2.3 x 2.4	moderate osteosclerosis; compact neural arch (spongious along its inner margin) large centrum cavity; spongious facets	pfb, unusual pfb, radial svc; moderate vascularity	aff. *Nothosaurus marchicus*
Wijk10-535 complete sacral	Winterswijk Anisian	1.95 x 1.65	moderate osteosclerosis; compact neural arch with large ventral cavities at each side; spongious	pfb, unusual pfb, radial svc; moderate vascularity	aff. *Nothosaurus marchicus*

This article has been accepted for publication and undergone full peer review but has not been through the copyediting, typesetting, pagination and proofreading process which may lead to differences between this version and the Version of Record. Please cite this article as doi: 10.1002/ar.24140

			centrum surrounded by a thin layer of compact cortex; spongious facets		
Wijk08-94 dorsal centrum	Winterswijk Anisian	0.96 x 1.15	moderate osteosclerosis; spongious facet; large cavity in centrum	pfb, radial svc; moderate vascularity	aff. *Nothosaurus marchicus*
Wijk08-111 dorsal centrum	Winterswijk Anisian	0.7 x 0.94	moderate osteosclerosis; spongious facet; large centrum cavity with endosteal trabeculae surrounded by thick compact cortex	highly organized pfb; radial and longitudinal svc; moderate vascularity	aff. *Nothosaurus marchicus*
Wijk08-47 longitudinal section of a dorsal centrum	Winterswijk Anisian	1.15 (length) x 0.875 (height)	moderate osteosclerosis; dorsal periost is compact, the rest spongious, moderately sized centrum cavity surrounded by thick compact cortex	pfb, radial and longitudinal svc; moderate vascularity	aff. ?*Nothosaurus marchicus*
Pachypleurosauria					
PIMUZ phz 161 incomplete dorsal	Mte S. Giorgio Anisian/Ladinian	nm	pachyosteosclerotic; ed filled centrum cavity; slightly spongious facets	pfb, radial svc, high vascularity	*Neustciosaurus edwardsii*
PIMUZ phz 160 neural arch	Mte S. Giorgio Anisian/Ladinian	nm	pachyosteosclerotic; small centrum cavity; slightly spongious facets	pfb, radial svc, high vascularity	*Neustciosaurus edwardsii*
PIMUZ T 4748 neural arch	Mte S. Giorgio Anisian/Ladinian	nm	extremely pachyosteosclerotic; compact cortex	pfb, radial svc, low vascularity	*Neustciosaurus edwardsii*
PIMUZ T 4757 complete dorsal	Mte S. Giorgio Anisian/Ladinian	nm	pachyosteosclerotic; compact cortex with a medium-sized centrum cavity; slightly spongious facets	pfb, radial svc, high vascularity	*Neustciosaurus edwardsii*
PIMUZ T 1568 complete dorsal	Mte S. Giorgio Anisian/Ladinian	nm	extremely pachyosteosclerotic; compact cortex; large compact medullary region	pfb-lb; very few radial scv; nearly avascular	*Serpianosaurus*
PIMUZ T 1565 centrum	Mte S. Giorgio Anisian/Ladinian	nm	extremely pachyosteosclerotic; compact cortex; large compact medullary region	avascular lb	*Serpianosaurus*
PIMUZ T 1564	Mte S. Giorgio	nm	extremely pachyosteosclerotic; compact cortex	pfb-lb; very few radial scv; nearly	*Serpianosaurus*

neural arch	Anisian/Ladinian			avascular	
PIMUZ T phz 90 neural arch	Mte S. Giorgio Anisian/Ladinian	nm	extremely pachyosteosclerotic; compact cortex; large compact medullary region	pfb-lb; few radial scv; low vascularity.	*Serpianosaurus*
Wijk08-99 dorsal centrum	Winterswijk Anisian	0.57 x 0.63	moderately osteosclerotic; spongious facet; large centrum cavity surrounded by thick layer of compact cortex	pfb, unusual pfb, radial and longitudinal svc; moderate vascularity	aff. *Anarosaurus*
Wijk08-126 caudal centrum	Winterswijk Anisian	0.35 x 0.54	moderately osteosclerotic; spongious facet; large centrum cavity surrounded by moderately sized compact cortex	pfb, unusual pfb, radial and longitudinal svc; moderate vascularity	aff. *Anarosaurus*
Eosauropterygia indet.					
Ribs					
Placodontia		**length**			
Wijk16- GG complete dorsal rib	Winterswijk Anisian	> 11.5	osteosclerotic; spongious medullary region	FLB; radial and longitudinal po; no remodeling; resorption of po	Placodontia indet.
Nothosauridae					
SMNS 80266 complete dorsal rib	Kupferzell Ladinian	nm	osteosclerotic; spongious medullary region	pfb, unusual pfb; mainly longitudinal po; resorption of po with incomplete remodeling; fibres	*Nothosaurus* sp.
SMNS 96928 dorsal rib (distal part)	Crailsheim Grenzbonebed	nm	osteosclerotic; compact medullary region surrounded by thin layer of compact cortex	pfb; nearly avascular compact cortex; remodeling in medullary regions, fibres	*Nothosaurus* sp.
SMNS 84371 complete dorsal rib	?	nm	osteosclerotic; free central cavity	high organized pfb; moderate vascularity, longitudinal pos; cavity lined by endosteal bone	*Nothosaurus* sp.
SMNS 84393 complete dorsal rib	?	nm	osteosclerotic; proximal (small) to medial (moderately sized) part with free cavity; distal part	high organized pfb; high vascularized, longitudinal & sheated po	*Nothosaurus* sp.

			with compact medullary region		
Wijk09-382 complete dorsal rib	Winterswijk Anisian	6 x nm	osteosclerotic; proximally small decentral free cavity; proximal to distal: spongious medullary region	pfb; nearly avascular; resorption; fibres	aff. *Nothosaurus marchicus*
PIMUZ phz 296 proximal part of dorsal rib	Mte S. Giorgio Anisian/Ladinian		pachyosteosclerotic; very small, decentral cavity surrounded by thick compact cortex	pfb; radial and longitudinal svc	*Ceresiosaurus*
PIMUZ T 5622 proximal to medial part of dorsal rib	Mte S. Giorgio Anisian/Ladinian	nm	pachyosteosclerotic; proximal part with small decentral free cavity; medial part with moderately sized compact medullary region	proximal: pfb; radial svc; medial: higher organized pfb-lb; low vascularity	*Ceresiosaurus*
PIMUZ T 5153 medial part of dorsal rib	Mte S. Giorgio Anisian/Ladinian	nm	pachyosteosclerotic; moderately sized compact medullary region	pfb; moderate vascularity	*Ceresiosaurus*
PIMUZ T 5454 medial part of dorsal rib	Mte S. Giorgio Anisian/Ladinian	nm	pachyosteosclerotic; large compact medullary region	pfb; high vascularity	*Ceresiosaurus*
Wijk07-31 complete dorsal rib	Winterswijk Anisian	~6.5 x nm	osteosclerosis; proximally to medially large to moderately sized free cavity; distal large spongious medullary region	highly organized pfb/lb; nearly avascular; fibers	?*Lariosaurus*
chypleurosauria					
PIMUZ phz 14 medial part of dorsal rib	Mte S. Giorgio Anisian/Ladinian	nm	pachyosteosclerotic; large compact medullary region	pfb; high vascularity; radial svc	*N. edwardsii*
PIMUZ T 4749 medial part of dorsal rib	Mte S. Giorgio Anisian/Ladinian	nm	pachyosteosclerotic; moderately sized compact medullary region	pfb; low vascularity; fibers	*N. edwardsii*
PIMUZ phz 163 proximal part of dorsal	Mte S. Giorgio Anisian/Ladinian	nm	pachyosteosclerotic; small, decentral free cavity	avascular pfb	*N. edwardsii*

rib					
PIMUZ T 4748 medial to distal part of dorsal rib	Mte S. Giorgio Anisian/Ladinian	nm	pachyosteosclerotic; medial (small) and distal (large) compact medullary region	low vascularity, highly organized pfb; short fibers & Sharpe's fibers	*N. edwardsii*
PIMUZ T 4752 medial to distal part of dorsal rib	Mte S. Giorgio Anisian/Ladinian	nm	pachyosteosclerotic; large compact medullary region	moderate vascularity (large longitudinal svc), pfb	*N. edwardsii*
PIMUZ T 1565 proximal part of dorsal rib	Mte S. Giorgio Anisian/Ladinian	nm	pachyosteosclerotic; proximally small decentral free cavity; medial: moderately sized compact medullary region	avascular pfb	*Serpianosaurus*
PIMUZ T 1564 medial part of dorsal rib	Mte S. Giorgio Anisian/Ladinian	nm	pachyosteosclerotic; moderately sized compact medullary region	avascular pfb	*Serpianosaurus*
PIMUZ T 1568 distal part of dorsal rib	Mte S. Giorgio Anisian/Ladinian	nm	pachyosteosclerotic; large compact medullary region	avascular pfb	*Serpianosaurus*
PIMUZ T 131 medial part of dorsal rib	Mte S. Giorgio Anisian/Ladinian	nm	pachyosteosclerotic; large compact medullary region	avascular pfb	*Serpianosaurus*
Wijk09-557 dorsal rib	Winterswijk Anisian	nm			aff. *Anarosaurus*
Wijk10-130 prox. to medial part of dorsal rib	Winterswijk Anisian	nm	osteosclerotic; proximally small decentral free cavity; medial moderately sized compact medullary region (endosteal bone)	inner cortex loosely organized pfb high vascularity; outer cortex high organized pfb, low vascularity to avascular	aff. *Anarosaurus*

Wijk09-37 medial part of dorsal rib	Winterswijk Anisian	nm X 3.51	osteosclerotic; large central free cavity	inner cortex loosely organized pfb high vascularity; outer cortex high organized pfb, low vascularity to avascular	aff. *Anarosaurus*
Eosauropterygia indet.					
SMNS 54434 complete dorsal rib	?	nm	osteosclerotic; proximally (small, decentral), medial (large central) and distal (enlarged) compact medullary region	moderate vascularity; pfb; mainly longitudinal svc & po	indet.
Wijk06-123 distal part of dorsal rib	Winterswijk Anisian	nm	osteosclerotic; moderately compact, enlarged medullary region	no primary cortex left	indet.
Wijk08-289 medial part of dorsal rib	Winterswijk Anisian	nm	osteosclerotic; moderately compact, enlarged medullary region	avascular pfb/lb; fibers	indet.
Gastralia					
SMNS 81882	Bayreuth	nm	osteosclerotic; moderately sized spongious medullary region	lb	*Nothosaurus*
PIMUZ T 4752	Mte S. Giorgio Anisian/Ladinian	nm	osteosclerotic; moderately sized compact medullary region	lb	*N. edwardsii*
PIMUZ T phz 158	Mte S. Giorgio Anisian/Ladinian	nm	osteosclerotic; compact small medullary region	lb	*N. edwardsii*
PIMUZ T 1568	Mte S. Giorgio Anisian/Ladinian	nm	osteosclerotic; moderately sized compact medullary region	lb	*Serpianosaurus*
SMNS 54413	?	nm	osteosclerotic; compact small medullary region	lb	Eosauropterygia *(*aff. *Nothosaurus)*
Wijk13-196	Winterswijk Anisian	nm	osteosclerotic; compact large medullary region	lb	Eosauropterygia (aff. *Anarosaurus*)

Wijk09-27	Winterswijk Anisian	nm	osteosclerotic; compact, very small medullary region	lb	Eosauropterygia (aff. *Anarosaurus*)

Table 2. Overview about microanatomical patterns in Sauropterygia and other marine reptiles. Please note that all centra of Sauropterygia vertebrae share a large central cavity (except in the pachypleurosaurs *Neusticosaurus* and *Serpianosaurus*), which is so far unique among amniotes. Information for the long bones are taken from other studies cited in the first column. Abbreviations: cc = calcified cartilage; po = primary osteons.

	long bones	**ribs**	**vertebrae**
(fast growing) Placodontia (Klein, 2010; Klein et al., 2015b)	BMI (& BMD) increased cortex thickness; high vascular density & primary trabecular structure; resorption of po but inhibition of remodeling; erosion of cc	BMI (& BMD) increased cortex thickness; high vascular density & primary trabecular structure; resorption of po but inhibition of remodeling	BMI (& BMD) increased cortex thickness; high vascular density & primary trabecular structure; resorption of po but inhibition of remodeling
Serpianosaurus mirigiolensis (Hugi et al., 2011)	extreme osteosclerosis /BMI increased cortex thickness; inhibition of remodeling; persistence of cc	extreme osteosclerosis /BMI change in distribution of periosteal and endosteal domain but retaining global compactness; inhibition of remodeling; persistence of cc	extreme osteosclerosis /BMI increased cortex thickness; inhibition of remodeling
Neusticosaurus edwardsii (Hugi et al., 2011; Klein and Griebeler, 2018)	osteosclerosis/BMI increased cortex thickness; inhibition of remodeling; persistence of cc	osteosclerosis/BMI change in distribution of periosteal and endosteal domain but retaining global compactness; inhibition of remodeling; persistence of cc	osteosclerosis/BMI increased cortex thickness; inhibition of remodeling
Anarosaurus heterodontus (Klein, 2010; Klein and	moderate osteosclerosis /BMI medium sized cavity surrounded by compact	osteosclerosis/BMI change in distribution of periosteal and	moderate osteosclerosis /BMI

Griebeler, 2018)	cortex	endosteal domain but retaining global compactness; persistence of cc in ribs and vertebrae but not in long bones at midshaft	
(small bodied) *Nothosaurus* sp. (Klein, 2010; Klein et al., 2016b)	moderate osteosclerosis /BMI medium sized cavity surrounded by compact cortex	osteosclerosis/BMI change in distribution of periosteal and endosteal domain but retaining global compactness; inhibition of remodeling; persistence of cc in ribs and vertebrae but not in long bones at midshaft	moderate osteosclerosis /BMI
(large bodied) *Nothosaurus* sp. (Krahl et al. 2013; Klein et al., 2016b)	thin-walled cortices to extreme osteosclerosis/ BMI, BMD increased and reduced cortex thickness; spongy resorption of periosteal bone; extreme enlargement of the medullary cavity	osteosclerosis/BMI change in distribution of periosteal and endosteal domain but retaining global compactness; inhibition of remodeling; persistence of cc in ribs and vertebrae but not in long bones at midshaft	cavernous structure /BMD
***Ceresiosaurus* sp.** (Hugi, 2011; Klein et al., 2016b)	extreme osteosclerosis/BMI increased cortex thickness; inhibition of remodeling	osteosclerosis/BMI change in distribution of periosteal and endosteal domain but retaining global compactness; inhibition of remodeling; persistence of cc	not studied
Simosaurus gaillardoti (Klein and Griebeler, 2016)	moderate osteosclerosis /BMI medium sized cavity surrounded by compact cortex	not studied	not studied